

## ON THE STELLAR COMPANION TO THE EXOPLANET HOSTING STAR 30 ARIETIS B

STEPHEN R. KANE<sup>1</sup>, THOMAS BARCLAY<sup>2,3</sup>, MICHAEL HARTMANN<sup>4</sup>, ARTIE P. HATZES<sup>4</sup>, ERIC L.N. JENSEN<sup>5</sup>, DAVID R. CIARDI<sup>6</sup>, DANIEL HUBER<sup>7,8</sup>, JASON T. WRIGHT<sup>9,10</sup>, ELISA V. QUINTANA<sup>2</sup>

*Submitted for publication in the Astrophysical Journal*

### ABSTRACT

A crucial aspect of understanding planet formation is determining the binarity of the host stars. Results from radial velocity surveys and the follow-up of *Kepler* exoplanet candidates have demonstrated that stellar binarity certainly does not exclude the presence of planets in stable orbits and the configuration may in fact be relatively common. Here we present new results for the 30 Arietis system which confirms that the B component hosts both planetary and stellar companions. Keck AO imaging provides direct detection of the stellar companion and additional radial velocity data are consistent with an orbiting star. We present a revised orbit of the known planet along with photometry during predicted transit times. Finally, we provide constraints on the properties of the stellar companion based on orbital stability considerations.

*Subject headings:* planetary systems – techniques: high angular resolution – techniques: radial velocities – techniques: photometric – stars: individual (30 Ari B)

### 1. INTRODUCTION

The binarity of stars is a topic of ongoing research, particularly in light of the plethora of exoplanets discovered over the past couple of decades. Exoplanets orbiting stars with a binary companions pose significant implications for formation theories, such as orbital stability (Holman & Wiegert 1999), and the period-mass (Zucker & Mazeh 2002) and period-eccentricity (Eggenberger et al. 2004) distributions. The searches for stellar companions to the host stars of *Kepler* exoplanet candidates has become an important component of the candidate validation process (Dressing et al. 2014; Everett et al. 2015; Wang et al. 2014). Attempts to detect binarity for the brightest exoplanet host stars are also underway (Crepp et al. 2012, 2013), and are often used to place constraints on additional planetary companions (Kane et al. 2014).

When it comes to multiplicity, one of the more exotic exoplanetary systems is that of 30 Arietis (hereafter 30 Ari). 30 Ari is a bound visual binary whose

main components are both main sequence F stars (F5V and F6V) separated by 38.1'' (1,500 AU). The A and B components are both relatively bright ( $V$  magnitudes of 6.48 and 7.09 respectively). 30 Ari A is a spectroscopic binary (Adams & Joy 1919; Morbey & Brosterhus 1974) with an orbital period of 1.1 days. 30 Ari B (HD 16232, HIP 12184, HR 764) was discovered by Guenther et al. (2009) to have a  $\sim 10 M_J$  companion with an orbital period of 335 days. The discovery was made using radial velocity (RV) observations which are not easy to undertake for such an early-type star, despite its brightness. The reason for this is that the spectra of early-type stars have a relatively small number of absorption lines and also tend to have rapid rotation rates, thus inhibiting precision RV measurements. The brightness of 30 Ari B in close proximity to the equally bright A component also proves problematic for photometric observations and so the system remained relatively unobserved for the years following the exoplanet discovery. Recently 30 Ari B was revisited using the adaptive optics capabilities of the Robo-AO system (Baranec et al. 2014) with target selection from the FG-67 database (Tokovinin 2014). The survey detected a stellar companion to the star (Riddle et al. 2015) that was further described by Roberts et al. (2015).

Here we present new observations of the 30 Ari B system that independently confirm the presence of a stellar companion in addition to the known planet orbiting the host star. Section 2 outlines the properties of 30 Ari B relevant to the subsequent analysis. Section 3 describes the detection of the stellar companion from Keck observations and the likelihood of the stars being bound. New RV and photometric data are presented in Section 4 which both are used to support the detection of the stellar companion and refine the properties of the known planet. Constraints on the physical and orbital properties of the stellar companion from these observations and orbital stability considerations are described in Section 5. We provide concluding remarks in Section 6 including a discussion of names for the system components.

skane@sfsu.edu

<sup>1</sup>Department of Physics & Astronomy, San Francisco State University, 1600 Holloway Avenue, San Francisco, CA 94132, USA

<sup>2</sup>NASA Ames Research Center, M/S 244-30, Moffett Field, CA 94035, USA

<sup>3</sup>Bay Area Environmental Research Institute, 596 1st Street West, Sonoma, CA 95476, USA

<sup>4</sup>Thüringer Landessternwarte, D-07778 Tautenburg, Germany

<sup>5</sup>Dept of Physics & Astronomy, Swarthmore College, Swarthmore, PA 19081, USA

<sup>6</sup>NASA Exoplanet Science Institute, Caltech, MS 100-22, 770 South Wilson Avenue, Pasadena, CA 91125, USA

<sup>7</sup>Sydney Institute for Astronomy (SIfA), School of Physics, University of Sydney, NSW 2006, Australia

<sup>8</sup>SETI Institute, 189 Bernardo Avenue, Mountain View, CA 94043, USA

<sup>9</sup>Department of Astronomy and Astrophysics, Pennsylvania State University, 525 Davey Laboratory, University Park, PA 16802, USA

<sup>10</sup>Center for Exoplanets & Habitable Worlds, Pennsylvania State University, 525 Davey Laboratory, University Park, PA 16802, USA

TABLE 1  
30 ARI B STELLAR PARAMETERS<sup>(1)</sup>

Parameter	Value
$J$	6.080
$V$	7.091
$B - V$	0.510
Proper motion ( $\alpha, \delta$ ) (mas) <sup>(2)</sup>	150.75, -12.79
Parallax (mas) <sup>(2)</sup>	$24.52 \pm 0.68$
Distance (pc) <sup>(2)</sup>	$40.8 \pm 1.1$
$M_*$ ( $M_\odot$ )	$1.16 \pm 0.04$
$R_*$ ( $R_\odot$ )	$1.13 \pm 0.03$

<sup>(1)</sup> Guenther et al. (2009) and references therein.

<sup>(2)</sup> van Leeuwen (2007)

## 2. HOST STAR PROPERTIES

This paper compiles imaging, RV, and photometric data of the 30 Ari system. The advantage of combining these datasets is to maximize constraints on both the kinematic and intrinsic luminosities of the component members. Determining these properties of the individual components depends heavily on the properties of 30 Ari B. The fundamental stellar properties of the star have been published numerous times in the literature, most recently by Tsantaki et al. (2014). In order to compile a self-consistent set of stellar parameters relevant to this work, and comparison with previous work on the planetary companion (see Section 4.1), we adopt those from van Leeuwen (2007) and Guenther et al. (2009), shown in Table 1. A particular reason for selecting these stellar parameters is to be consistent with the previous RV measurements of Guenther et al. (2009) such that a direct comparison of the Keplerian orbital solutions may be made (see Section 4).

## 3. DETECTION OF A STELLAR COMPANION

Shown in Figure 1 (left) is an  $\sim 9'$  FOV image of the 30 Ari visual binary extracted from the Digital Sky Survey<sup>11</sup>, centered on the A component. Our observations of 30 Ari B were acquired using NIRC2 with the AO system at Keck during the night of August 9th, 2014. We used the standard AO configuration for NIRC2 imaging observations, the details of which may be found in the NIRC2 Observer's Manual<sup>12</sup>. Sky conditions were poor (thin cirrus clouds) but sufficient to complete the observations given the brightness of the target. The camera was used in the narrow camera mode with a  $J$ -band filter. A total of nine 0.2 second exposures were acquired and co-added to produce a combined smoothed frame from which to conduct the analysis. The sensitivity of the observations to fainter stellar companions is demonstrated in Figure 2 which shows the  $5\sigma$  detection limit as a function of radial separation from the host star.

The combined Keck image is shown in Figure 1 (right). 30 Ari B is at the center of the frame and the stellar companion is plainly visible to the right of the host star. Measurements of the stellar profile centroids and the NIRC2 pixel scale ( $0.009942''/\text{pixel}$ ) show that the stars are separated by  $0.536''$ . The uncertainty in the  $X$ -direction is 0.646 pixels, equivalent to  $0.00642''$  or 6.42 mas in RA.

Similarly the uncertainty in the  $Y$ -direction is 0.245 pixels, equivalent to  $0.00244''$  or 2.44 mas in Dec. Thus the separation of the stars is  $0.536'' \pm 0.007''$  with a position angle of  $-73.6^\circ \pm 0.1^\circ$  (east of north).

The relative photometry between the two stars was estimated into two ways and the results compared. Because of the poor seeing on the night of the observations, there was not a clean centralized peak of the primary. To aid in the photometry, the final image was convolved with a 2-D circularly symmetric gaussian with the full-width set to 4 pixels: approximately half the full-width of the measured PSF. The first estimate utilized aperture photometry on each star where the aperture radius was set to the half-width of the convolved PSF (5 pixels). The second estimate was performed by fitting a 2-D gaussian to each of the stellar PSFs and subtracting the gaussians from the image until the residuals were minimized. The total flux in the gaussian PSFs were used to estimate the relative magnitudes of stars. The final relative photometry was determined from an average of the two methods, and the difference in the two methods was added in quadrature to the formal statistical uncertainties in the aperture and psf photometry. We find that the magnitude difference between the two stars  $\Delta_J = 3.15 \pm 0.07$ . Using the distance estimate of Table 1 leads to a projected separation of  $21.9 \pm 0.7$  AU and a companion absolute  $J$  magnitude of  $6.18 \pm 0.09$ . This is consistent with the companion being a late-type dwarf with an approximate spectral type of M1-3 (Boyajian et al. 2012).

The issue remains as to whether the detected companion is indeed gravitationally bound to the host star. No astrometric motion was detected through the analysis of *Hipparcos* data by Reffert & Quirrenbach (2011). This null-detection is not surprising however considering that the orbital period of the stellar companion is much longer than the time baseline of the *Hipparcos* observations. The proper motion of 30 Ari B according to van Leeuwen (2007) is  $0.151'' \pm 0.00075''$ . The astrometric results of Roberts et al. (2015) confirm that the newly detected companion to 30 Ari B has a common proper motion, increasing the likelihood that they are bound. To investigate this further, we adopt the statistical validation techniques described Horch et al. (2014). The  $5\sigma$  detection limit shown in Figure 2 is similar to the detection limit achieved with the Differential Speckle Survey Instrument (DSSI) on Gemini-North, shown in Figure 9 of Horch et al. (2014). Linear interpolation of the figure bins indicates that the likelihood of our detected companion being bound to 30 Ari B is  $> 82\%$ . However, the observations of Horch et al. (2014) were of the *Kepler* field which has a higher density of stars. To account for that, we used the TRILEGAL code<sup>13</sup> (Girardi et al. 2005) to determine the relative number of stars along the respective lines-of-sight for 30 Ari B and the *Kepler* field. A 1 square degree search with the TRILEGAL model yields 16,210 line-of-sight companions for 30 Ari B and 167,936 line-of-sight companions for the *Kepler* field ( $l = 76.53$ ,  $b = 13.29$ ). Assuming the binarity rate does not change, the probability that the companion detected near 30 Ari B is gravitationally bound is increased by the ratio of the number of companions predicted, which is a factor of  $\sim 10$ . Thus, the probability that the detected

<sup>11</sup> [https://archive.stsci.edu/cgi-bin/dss\\_form](https://archive.stsci.edu/cgi-bin/dss_form)

<sup>12</sup> <http://www2.keck.hawaii.edu/inst/nirc2/Manual/ObserverManual.html>

<sup>13</sup> <http://stev.oapd.inaf.it/cgi-bin/trilegal>

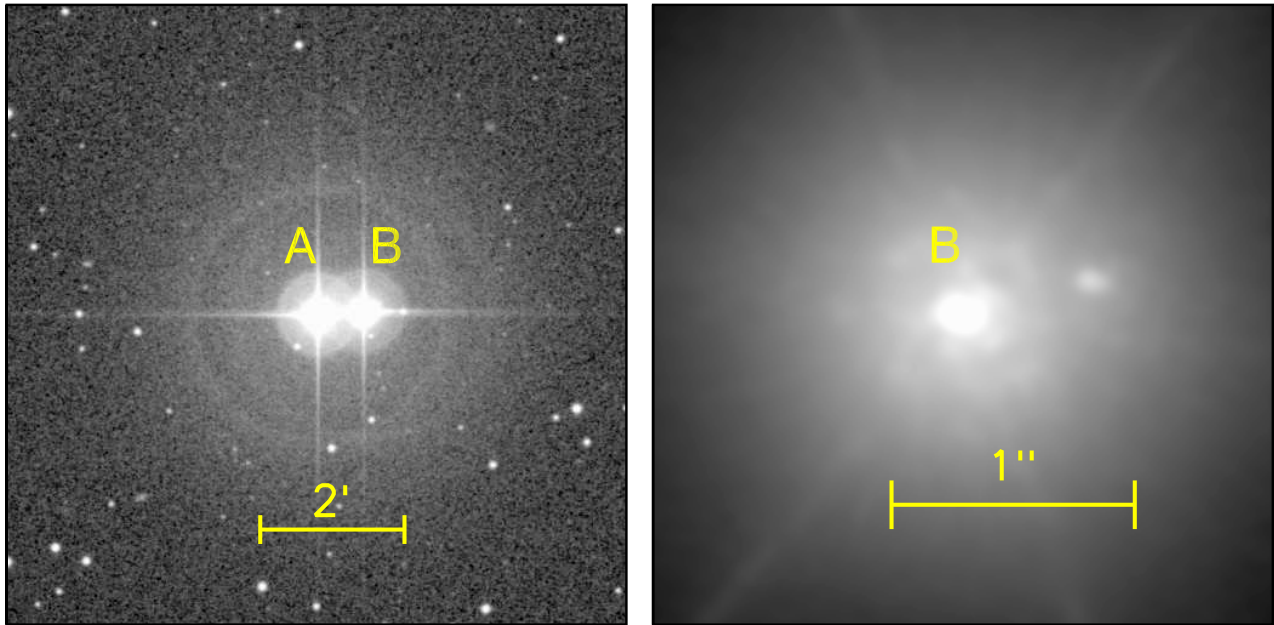


FIG. 1.— Images of the 30 Ari system from the Digital Sky Survey (Left) and Keck observations (right). In both cases the field orientation is up-North and left-East. Left: Image of the 30 Ari system centered on the A component. Right: Keck/NIRC2 combined image of 30 Ari B showing the presence of the stellar companion.

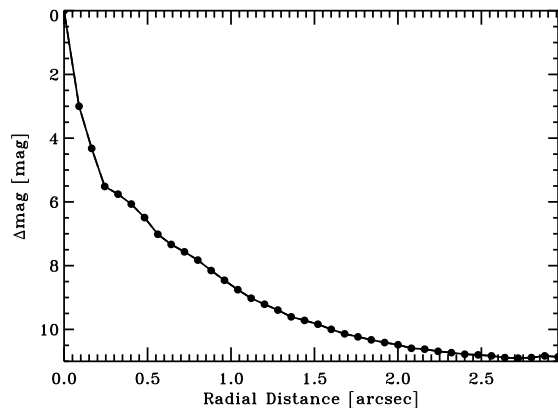


FIG. 2.— The  $5\sigma$  Keck image sensitivity (in units of  $\Delta$  magnitude) as a function of separation from the host star.

companion is bound to 30 Ari B is  $\sim 100\%$ .

At the point of submitting this work, we learned that the stellar companion to 30 Ari B has also been detected by the Robo-AO team (Riddle et al. 2015). We present the Keck AO component of these results as an independent detection of this companion. Their observations were conducted using an  $i$  filter and reveal a similar angular separation of  $0.536''$ . If the detected companion is gravitationally bound, the 30 Ari B components should have colors and absolute magnitudes that are compatible with stellar isochrones. To test this, we combine the  $J$ -band detection from our Keck observations with the  $i$ -band detection from Robo-AO to place the components on a color-magnitude diagram.

The available  $i$ -band photometry of 30 Ari B from the Sloan (Ahn et al. 2012) and APASS<sup>14</sup> surveys is heavily saturated, and therefore not reliable for this system. To

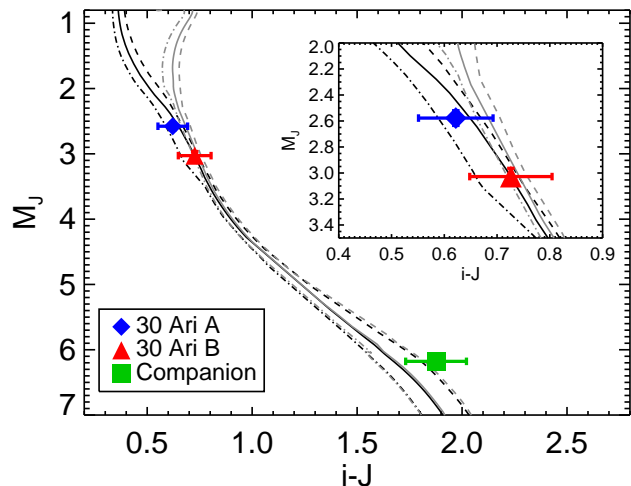


FIG. 3.— 0.5 Gyr (black) and 1.5 Gyr (gray) Dartmouth stellar isochrones with  $[\text{Fe}/\text{H}] = -0.1$  (dash-dotted lines), 0.1 (solid lines) and 0.3 (dashed lines). Note that the 0.5 Gyr isochrone has been obtained by linearly interpolating the original  $< 1$  Gyr isochrone grid available in the Dartmouth database. The inset shows a zoom on the position of 30 Ari A and B.

derive an approximate  $i$  magnitude, we fit  $J-K$  and  $M_J$  to a grid of Dartmouth isochrones (Dotter et al. 2008) assuming zero reddening, which is justified by the relatively small distance ( $\sim 41$  pc) to the system. The metallicity of the 30 Ari system is poorly constrained, with values ranging from near solar metallicity from Stromgren photometry (Casagrande et al. 2011) to  $[\text{Fe}/\text{H}] \sim +0.27$  from various spectroscopic studies (see Guenther et al. 2009, and references therein). Adopting a metallicity prior of  $[\text{Fe}/\text{H}] = 0.1 \pm 0.2$  for the isochrone fit, which approximately corresponds to the central value and spread of the quoted literature values, we derive a synthetic absolute magnitude of  $M_i = 3.75 \pm 0.08$  mag for 30 Ari B. Combining this with  $\Delta J = 3.15 \pm 0.07$  mag and

<sup>14</sup> <http://www.aavso.org/apass>

$\Delta i = 4.2 \pm 0.1$  mag, the corresponding colors are  $i - J = 0.73 \pm 0.08$  mag for 30 Ari B and  $i - J = 1.88 \pm 0.13$  mag for the detected stellar companion, respectively.

Figure 3 compares the positions of 30 Ari B and the detected companion in a  $M_J$ ,  $i - J$  color-magnitude diagram to 0.5–1.5 Gyr isochrones for a range of metallicities. 30 Ari A is also shown, with an  $i - J$  color derived using the same procedure as described above. The comparison shows that all three components have colors that are consistent with a given distance modulus, and hence are compatible with being in a gravitationally bound system.

#### 4. RADIAL VELOCITIES AND PHOTOMETRY

Here we present new RV and photometric data of 30 Ari B in support of our observations of the stellar companion.

##### 4.1. Revised Planetary Parameters and Linear Trend

The RV dataset for 30 Ari B published by Guenther et al. (2009) consisted of 98 measurements and revealed the presence of a sub-stellar companion in a 335 day orbit around the host star. Guenther et al. (2009) did not provide a fit that included a linear trend free parameter since the presence of such a trend was negligible in those data. Here we provide 12 additional measurements which extend the time baseline by  $\sim 300$  days and thus greater sensitivity to the possible influence of a stellar companion. The data were acquired from continued observations 2m Alfred Jensch telescope of the Thüringer Landessternwarte Tautenburg, described in detail by Hatzes et al. (2005), and were reduced with the same data pipeline as for those for Guenther et al. (2009). The data were modeled using a partially linearized, least-squares fitting procedure (Wright & Howard 2009). Parameter uncertainties were estimated using the BOOTTRAN bootstrapping routines developed by Wang et al. (2012). The new best-fit Keplerian orbital solution is shown in Table 2 and Figure 4 along with the fit residuals. The parameters include orbital period ( $P$ ), time of periastron passage ( $T_p$ ), eccentricity ( $e$ ), periastron argument ( $\omega$ ), RV semi-amplitude ( $K$ ), minimum planet mass ( $M_p$ ), semi-major axis ( $a$ ), and the RV linear trend ( $dv/dt$ ). The complete set of new and revised 110 RV measurements are provided in Table 3.

There are several notable changes over the orbital solution of Guenther et al. (2009), shown in Table 2. The inclusion of a linear trend is warranted by the extended baseline and the solution shows that the trend is significant at the  $4\sigma$  level. The linear trend has consequences for the Keplerian solution in that the orbital period is slightly increased and the “shape” of the orbit (eccentricity and periastron argument) is less well constrained since it is closer to being circular. Another change of note is that the linear trend partially compensates for the semi-amplitude of the RV variations resulting in a smaller minimum mass for the sub-stellar companion of  $6.6 M_J$ . The companion in question is thus more likely to be planetary in nature than an object in the brown dwarf regime. Finally, it should be noted that we have not excluded any of the significant RV outliers (e.g., the measurement acquired at epoch 2,452,655.25, see Table 3). Testing such exclusions did not significantly impact the

Keplerian orbital solution. The implications of the linear trend for the detected stellar companion to 30 Ari B are discussed in more detail in Section 5.1.

TABLE 3  
30 ARI B RADIAL VELOCITIES

Date (JD - 2,450,000)	RV ( $\text{m s}^{-1}$ )	$\sigma$ ( $\text{m s}^{-1}$ )
2515.600993	754.1050	229.87
2545.536478	220.9028	250.29
2545.544754	192.3126	210.82
2548.472892	421.2561	121.74
2571.576275	336.9965	132.71
2592.467015	479.7458	141.60
2596.415295	307.9014	114.94
2655.252792	-888.2267	319.81
2656.242768	-232.6306	206.70
2657.267185	-168.8275	214.44
2659.260606	-255.4376	246.96
2660.294048	-178.7523	318.83
2662.268544	79.8795	225.79
2681.341841	-219.0311	300.12
2714.276746	-96.3552	320.68
2834.523535	107.0504	156.15
2858.575149	275.5233	160.05
2859.600468	326.0843	148.02
2861.586390	156.6134	110.20
2863.588342	340.7115	180.12
2878.477610	277.3908	171.12
2925.422421	193.6456	129.42
2926.480403	190.0219	148.87
2931.400890	343.9288	109.36
2948.365052	213.9280	164.54
2949.384915	196.2251	150.77
2950.438364	134.0650	191.77
2950.444684	80.5700	179.43
2952.400062	-131.2379	192.41
2955.422149	419.4916	172.12
2956.465067	303.5786	121.07
2981.367219	-21.7257	107.85
2982.388335	129.1056	153.39
2983.413199	84.5132	99.35
3022.290291	-409.6576	332.74
3023.367630	-183.1904	221.21
3076.292073	135.4815	453.15
3221.496697	197.4571	186.82
3224.547386	260.7274	167.63
3225.512468	229.8522	137.80
3247.392319	537.8008	284.92
3248.490970	4.2384	142.16
3250.480289	327.6601	156.85
3251.466370	60.7189	145.38
3252.492894	250.7651	114.60
3253.432338	337.5163	161.58
3254.450110	280.9421	148.70
3275.513744	292.7484	119.60
3277.546322	112.2383	164.09
3280.508460	165.4369	150.31
3281.621507	105.3440	133.67
3282.493267	85.4409	168.59
3284.350643	126.1022	200.37
3301.371752	202.2588	169.87
3309.444008	100.2754	138.43
3388.344614	-364.0933	323.23
3431.291948	-349.9726	285.70
3432.265935	-338.8958	263.92
3658.364855	-140.6013	137.69
3662.535227	-62.5995	142.97
3749.258017	-480.4116	259.14
3780.366708	-433.3393	235.41
3783.265338	-286.6540	231.20
3784.288850	-254.0487	275.03
3814.276631	152.9526	165.55
3815.290494	-186.8709	150.55
3954.589497	-63.4947	137.82
3985.625596	-45.7626	147.38
4018.454970	-65.4861	99.70
4070.394848	60.2101	117.30

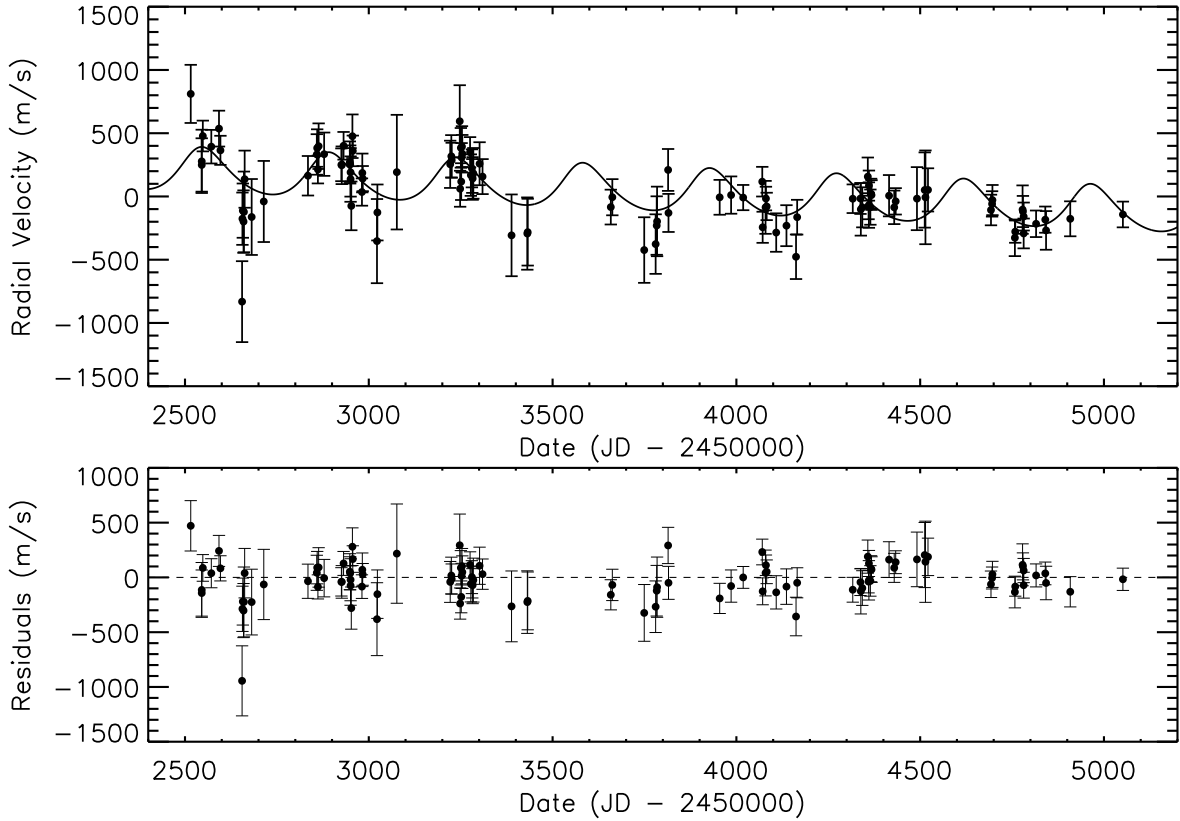


FIG. 4.— All 110 RV measurements of 30 Ari B acquired using the 2m Alfred Jensch telescope (see Table 3). Top: The new orbital solution including a linear trend due to the presence of the stellar companion, provided in Table 2. Bottom: The RV residuals (observed minus computed) from the best-fit model.

TABLE 2  
KEPLERIAN ORBITAL MODEL

Parameter	Value (Guenther et al. 2009)	Value (This work)
30 Ari B b		
$P$ (days)	$335.1 \pm 2.5$	$345.4 \pm 3.8$
$T_p$ (JD - 2,440,000)	$14538 \pm 20$	$13222.1 \pm 42.4$
$e$	$0.289 \pm 0.092$	$0.18 \pm 0.11$
$\omega$ (deg)	$307 \pm 18$	$337 \pm 57$
$K$ ( $\text{m s}^{-1}$ )	$272 \pm 24$	$177 \pm 26$
$M_p \sin i$ ( $M_J$ )	$9.88 \pm 0.94$	$6.6 \pm 0.9$
$a$ (AU)	$0.995 \pm 0.012$	$1.01 \pm 0.01$
$dv/dt$ ( $\text{m/s/day}$ )	0.0	$-0.12 \pm 0.03$
System Properties		
$\gamma$ ( $\text{m s}^{-1}$ )	-	$9.8 \pm 17.7$
Measurements and Model		
$N_{\text{obs}}$	98	110
rms ( $\text{m s}^{-1}$ )	135	181.5
$\chi^2_{\text{red}}$	-	0.82

TABLE 3 — Continued

Date (JD - 2,450,000)	RV ( $\text{m s}^{-1}$ )	$\sigma$ ( $\text{m s}^{-1}$ )
4071.515854	-300.3802	122.88
4079.374428	-142.8664	209.14
4080.365276	-73.1703	93.38
4082.438154	-135.5155	108.22
4108.340755	-342.0903	151.94
4136.254291	-287.5546	161.89
4162.258663	-533.4807	176.15

TABLE 3 — Continued

Date (JD - 2,450,000)	RV ( $\text{m s}^{-1}$ )	$\sigma$ ( $\text{m s}^{-1}$ )
4165.348658	-220.5430	137.41
4316.580289	-74.6582	113.25
4337.564193	-73.0027	121.86
4338.559366	-158.5779	207.82
4342.615233	-142.4315	158.33
4357.560127	100.1291	151.16
4359.572735	-133.7737	103.00

TABLE 3 — *Continued*

Date (JD - 2,450,000)	RV ( $\text{m s}^{-1}$ )	$\sigma$ ( $\text{m s}^{-1}$ )
4360.541338	-124.8448	179.69
4360.576121	29.2391	118.99
4364.560715	-141.0313	139.21
4366.536859	-34.9721	118.68
4367.554451	-45.7453	117.28
4415.427584	-50.7634	163.37
4429.384583	-142.7605	132.56
4433.367364	-95.2091	104.31
4491.292838	-73.9298	249.26
4512.358374	-5.8152	297.29
4514.353088	-63.6416	370.58
4521.285415	-4.7234	170.85
4692.598912	-163.7491	120.98
4695.601537	-115.6291	100.32
4696.539080	-85.1723	119.14
4757.636700	-383.5377	144.69
4758.610225	-334.8741	87.91
4778.588013	-160.5203	191.33
4779.531238	-175.7052	123.25
4781.531450	-215.3962	110.56
4781.573376	-349.1836	118.00
4815.330030	-272.7974	104.98
4840.347284	-239.8999	103.61
4842.460148	-325.0461	152.85
4908.311715	-233.2704	138.19
5051.539182	-199.2144	101.76

#### 4.2. Potential Planetary Transit

With the detection of the low-mass stellar companion to 30 Ari B, we undertook the task of acquiring photometry that may have indications of stellar variability. Variability studies of *Kepler* stars have shown that F-type stars tend to have much shorter variation periods, likely due to pulsations rather than the activity typical of low-mass stars (Ciardi et al. 2011; McQuillan et al. 2012).

The first photometric data source we examined was the photometry from the *Hipparcos* mission, shown in the top panel of Figure 5. These data demonstrate photometric stability at the  $\sim 1\%$  level. However, there are two significant outliers in the photometry indicating an  $\sim 5\%$  reduction in brightness of the host star. The most intriguing aspect of these two outliers is that they are separated by  $\sim 693.8$  days - approximately twice the revised orbital period of the planet (see Section 4.1). If such variation were indeed due to the passage of the planet across the stellar disk, the depth appears to be too large. Additionally, the probability of the transit being detected in the sparsely sampled *Hipparcos* data is extremely low. Nevertheless, to investigate this further, we constructed a transit ephemeris based upon the *Hipparcos* photometry since these data yield greater timing precision than predictions based upon the RV data described in Section 4.1.

30 Ari B was observed using the 0.6m telescope at the Peter van de Kamp Observatory, Swarthmore College on the nights of November 15th and 16th, 2014. Observations were conducted in good weather conditions using an r' filter and 10 second exposures. 30 Ari A provided a natural comparison star from which to perform relative photometry since it is similar in both brightness and color. Based upon the *Hipparcos* dips, a possible event was predicted for a JD of around 2,456,976. These data

are shown in the middle and bottom panels of Figure 5. Though no event similar to that seen in the *Hipparcos* data was detected, the star was observed to be consistently stable at the level of a couple of millimag. These data also rule out significant stellar pulsations of periods less than  $\sim 6$  hours. It is certainly possible that the outlier measurements in the *Hipparcos* dataset are simply spurious, but the curious coincidence with the orbital period of the planet leads us to encourage continued observations.

#### 5. ORBITAL DYNAMICS OF THE COMPANION

The properties of the stellar companion may be further constrained from orbital dynamics considerations, as we describe in this section.

##### 5.1. Mass and Orbit

The mass and separation of the stellar companion to 30 Ari B may be constrained from the linear trend detected in the RV data (see Section 4.1). The trend does not exhibit a “turn-around” point where the slope changes from negative to positive. However, the total amplitude of the trend over the time baseline of the observations places a lower limit on the semi-amplitude of the variations due to the companion. The trend shown in Table 2 multiplied by the time baseline (2,536 days) yields a minimum RV amplitude of  $\sim 305 \text{ m s}^{-1}$ .

The left panel of Figure 6 shows the resulting mass/separation limits where the linear trend has been converted to an acceleration,  $\dot{v}$  and then converted to a mass estimate via  $M_B = (\dot{v}a^2)/G$  where  $\dot{v} = dv/dt$ ,  $M_B$  is the mass of the detected binary companion, and we have assumed a circular orbit. The limit is shown as a solid line and the dashed lines represent the  $1\sigma$  uncertainties propagated from the linear trend uncertainties. Anything below these lines has either insufficient mass or proximity to the host star to produce the observed trend. Since we know from the angular separation (see Section 3) that the companion semi-major axis is at least 21.9 AU (vertical dotted line), the companion lower mass limit is  $\sim 27$  Jupiter masses. The valid area of parameter-space shown in the figure may thus be constrained to the shaded region.

An additional constraint on the companion mass may be applied by extending the above methodology, as described by Howard et al. (2010). The physical separation between the 30 Ari B stars, if they are bound, is  $21.9 \text{ AU} / \sin(\theta)$  where  $\theta$  is the angle between our line-of-sight and the primary-secondary vector ( $\theta = 0$  implies the secondary is behind the primary). If the secondary is the source of the RV linear trend described in Section 4.1, then it imparts a line-of-sight acceleration of  $\dot{v} = (GM_B/r^2) \times \cos(\theta)$  where  $r$  is the physical separation with no assumption regarding orbital eccentricity. This leads to the following expression for the companion mass:

$$M_B = \frac{\dot{v}(21.9 \text{ AU})^2}{G(1 - \cos^2(\theta)) \cos(\theta)} \quad (1)$$

The cubic term in the denominator must be negative since  $dv/dt$  is negative and  $M_B$  is positive. Furthermore, because the cosine function is bound between -1 and 1, the cubic's value lies between -0.385 and zero. The equa-

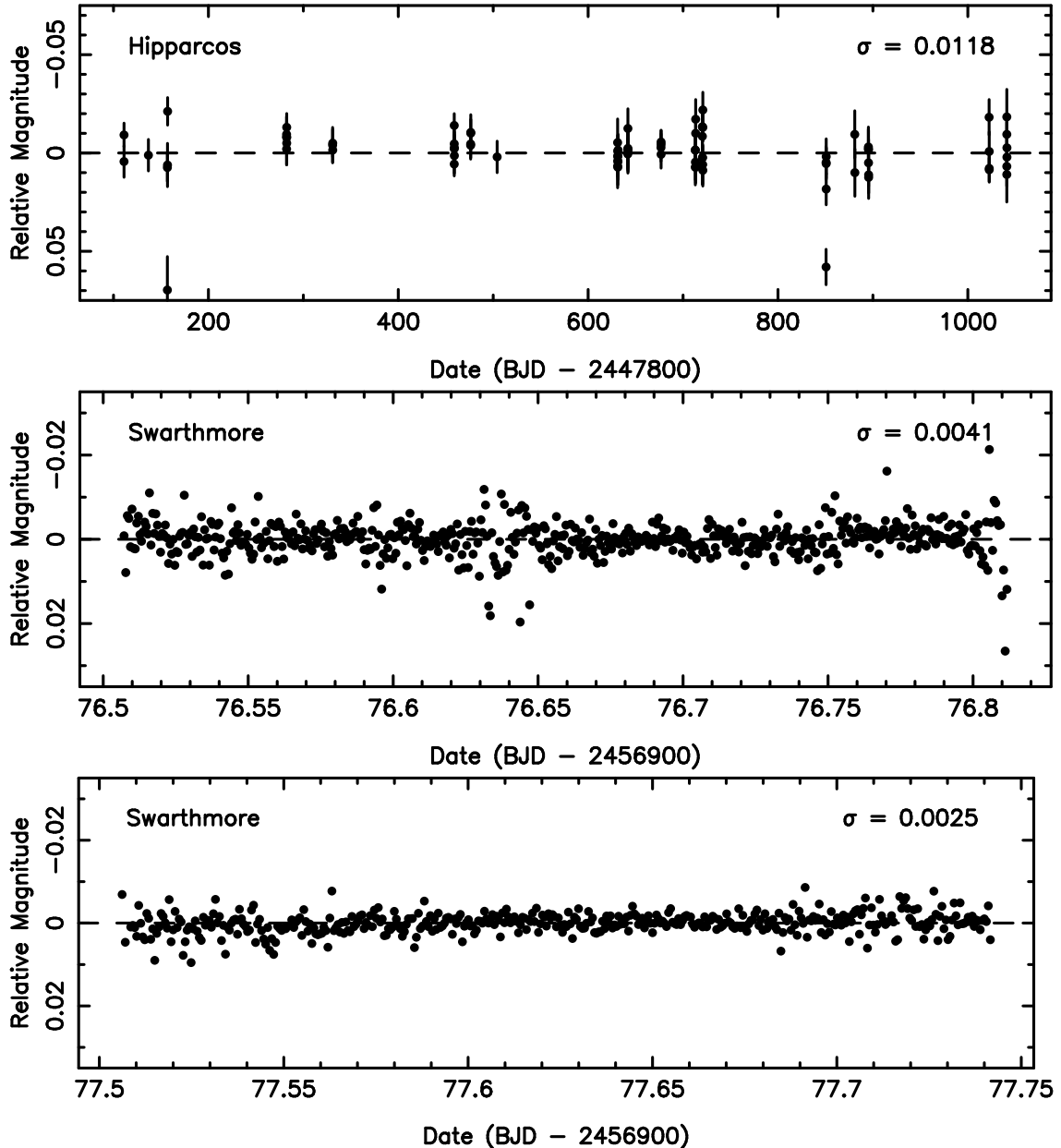


FIG. 5.— Photometry of 30 Ari B from the *Hipparcos* mission (top panel) and the Swarthmore 0.6m telescope (middle and bottom panels). The number in the top-right of each panel is the  $1\sigma$  rms scatter of the data points. Though no transit events were observed in the Swarthmore data, the star was found to be photometrically stable within a couple of millimag. Note the different vertical axis scales between the *Hipparcos* and Swarthmore plots.

tion therefore becomes an inequality for  $M_B$ :

$$M_B > \frac{(-0.12 \pm 0.03 \text{ m/s/day}) \times (21.9 \pm 0.7 \text{ AU})^2}{G(-0.385)} \quad (2)$$

where we have substituted the linear trend from Table 2. This results in a minimum mass of the stellar companion of  $M_b > 0.29 \pm 0.08 M_\odot$ , consistent with the companion being M1-3 as determined in Section 3.

The calculated properties of the companion, including the mass of 30 Ari B and the projected separation, result in a minimum orbital period of  $95 \pm 6$  years. This is consistent with the companion being of stellar mass producing an observed long timescale RV trend.

## 5.2. System Orbital Stability

The existence of a planet located  $\sim 1$  AU from the host star may be used to place further constraints on the orbit of the stellar companion. Planets have been detected in both S-type and P-type orbits, the stability of which have been investigated by numerous authors (Harrington 1977; Eggleton & Kiseleva 1995; Musielak et al. 2005). We use the analytical solutions provided by Holman & Wiegert (1999) to determine the range of binary separations and eccentricities that will allow the planetary orbit to remain stable. To do this, we invert Equation 1 of Holman & Wiegert (1999) as fol-

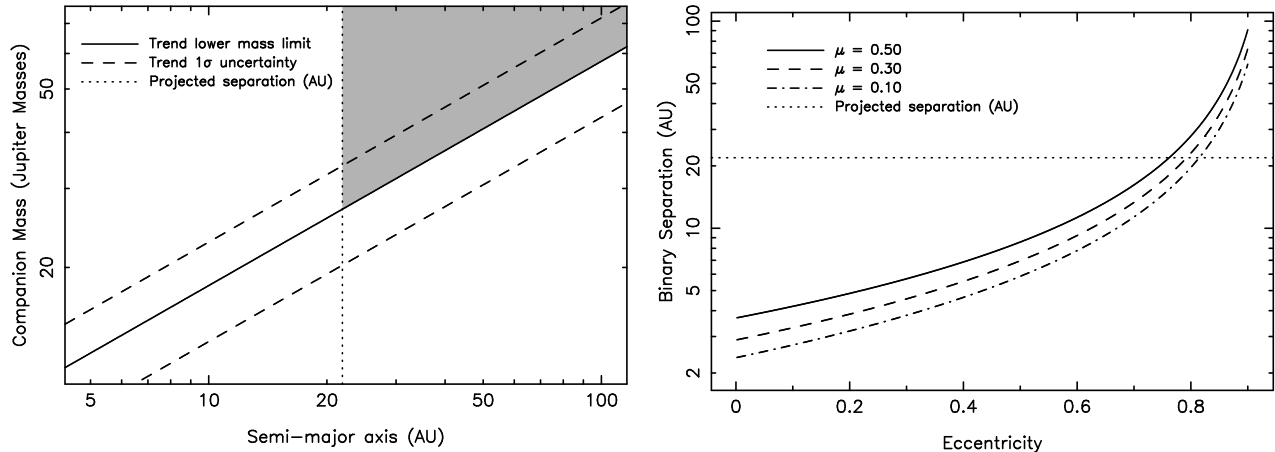


FIG. 6.— Limits on the properties of the companion star based on RV variations and stability constraints. Left: The lower mass limit for the stellar companion (solid line) imposed by the magnitude of the linear trend (assuming a circular orbit). The dashed lines are the  $1\sigma$  uncertainties and the vertical dotted line is the minimum projected separation (see Section 3). The shaded area is the valid region based on these constraints. Right: The minimum separation of the 30 Ari B binary components as a function of their orbital eccentricity that will allow the known planet to remain in a stable orbit. The horizontal dotted line represents the minimum projected separation of the stellar companion and the mass ratio is  $\mu \sim 0.3$ . Thus, the valid region of the plot is above both the dotted and dashed lines.

lows

$$a_b = a_c / [(0.464 \pm 0.006)] + (-0.380 \pm 0.010)\mu \\ + (-0.631 \pm 0.034)e + (0.586 \pm 0.061)\mu e \\ + (0.150 \pm 0.041)e^2 + (-0.198 \pm 0.074)\mu e^2 \quad (3)$$

where  $a_b$  is the binary separation,  $e$  is the binary orbital eccentricity, and  $a_c$  is the maximum allowed semi-major axis of the planet. The mass ratio,  $\mu$ , is defined as  $\mu = m_2/(m_1 + m_2)$ , and is thus  $\mu = 0.5$  for an equal mass binary. The right panel of Figure 6 shows the binary separation and eccentricity limitations for three different mass ratios with the constraint that a planet must be allowed to exist at  $a_c = 1.01$  AU. We have the additional constraint imposed by the projected separation of 21.9 AU, represented by the horizontal dotted line. Based on our spectral type estimate of M1, we adopt a mass for the companion of  $0.5 M_\odot$  resulting in a mass ratio of  $\mu = 0.3$ . Thus, the valid regions of the plot exist above both the dotted and dashed lines. For a companion separation equal to the projected separation, the eccentricity of the binary orbit must be less than  $\sim 0.75$ .

TABLE 4  
SUMMARY OF STELLAR COMPANION PROPERTIES

Parameter	Value	Section
Angular Separation (")	$0.536 \pm 0.007$	3
Projected Separation (AU)	$21.9 \pm 0.7$	3
$\Delta J$ magnitude	$3.15 \pm 0.07$	3
Apparent $J$ magnitude	$9.23 \pm 0.07$	3
Absolute $J$ magnitude	$6.18 \pm 0.09$	3
Spectral type	M1-3	3
RV linear trend (m/s/day)	$-0.12 \pm 0.03$	4.1
Mass ( $M_\odot$ )	$> 0.29 \pm 0.08$	5.1
Orbital Period (years)	$< 95 \pm 6$	5.1
Orbital Eccentricity ( $a_b = 21.9$ AU)	$< 0.75$	5.2

## 6. CONCLUSIONS

In this paper, we have presented significant new observations that attempt to describe the detected objects

orbiting 30 Ari B. Table 4 summarizes our derived parameters of the stellar companion to 30 Ari B. The 30 Ari system as a whole is clearly quite complex with the A and B components harboring planetary and stellar companions. This complexity may be attributed partially to the relative youth of the system since A and B are each less than 1 Gyr in age (Guenther et al. 2009), although the hierarchical structure of the system is likely stable for long timescales. Additionally, the relatively large (minimum) separation of the detected stellar companion to 30 Ari B produces orbital motion that makes it difficult to constraint the orbital inclination. If the companion and the known planet are coplanar then that would have significant implications for the formation and evolutionary history of the system and provide additional constraints on the overall system stability. Further observations of the companion will be able to improve our knowledge of the inclination and the kinematics of the system.

The rather unusual nature of the system as described raises the issue of appropriate system component names. The reader will have noticed that we have thus far avoided assigning a name to the companion. The nomenclature of such systems is as complex as the system itself, an example of which is described by Wright et al. (2013). One possibility, that uses binary star and exoplanet naming conventions, would be to rename the primary and secondary components of 30 Ari B to 30 Ari BA and 30 Ari BB respectively, leading to a corrected name for the planetary companion of 30 Ari BA b. The guidelines of the Washington Multiplicity Catalog standard (Raghavan et al. 2010) recommends that the stellar components of 30 Ari B be named 30 Ari Ba and 30 Ari Bb, leading to a collision with the planet naming convention. A compromise would be to name the newly-detected companion 30 Ari C (also advocated by Roberts et al. (2015)), allowing the planet to remain as 30 Ari Bb. This would avoid having a name-change for the planet change, which is desirable from a literature paper-trail perspective. We propose to adopt this latter as a provisional



naming convention for the system, as also adopted by Riddle et al. (2015). As it seems that many of the exoplanet host stars are part of binary systems, we can look forward to further discussion and adjustment of names and orbital parameters in the years ahead.

#### ACKNOWLEDGEMENTS

The authors would like to thank Elliott Horch, Steve Howell, and Suvrath Mahadevan for several useful discussions. Thanks are also due to the anonymous referee whose helpful comments improved the manuscript. D. Huber acknowledges support by the Australian Research Council's Discovery Projects funding scheme (project number DE140101364) and by NASA under Grant NNX14AB92G issued through the Kepler Participating Scientist Program. E.V. Quintana is supported by a NASA Senior Fellowship at the Ames Research Cen-

ter, administered by Oak Ridge Associated Universities through a contract with NASA. This work made use of the Digitized Sky Survey (DSS) hosted by the Mikulski Archive for Space Telescopes (MAST). This work was supported by a NASA Keck PI Data Award, administered by the NASA Exoplanet Science Institute. Data presented herein were obtained at the W. M. Keck Observatory from telescope time allocated to the National Aeronautics and Space Administration through the agency scientific partnership with the California Institute of Technology and the University of California. The Observatory was made possible by the generous financial support of the W. M. Keck Foundation. The authors wish to recognize and acknowledge the very significant cultural role and reverence that the summit of Mauna Kea has always had within the indigenous Hawaiian community. We are most fortunate to have the opportunity to conduct observations from this mountain.

#### REFERENCES

- Adams, W.S., Joy, A.H. 1919, *ApJ*, 49, 186  
 Ahn, C.P., Alexandroff, R., Allende Prieto, C., et al. 2012, *ApJS*, 203, 21  
 Baranec, C., Riddle, R., Law, N.M., et al. 2014, *ApJ*, 790, L8  
 Boyajian, T.S., von Braun, K., van Belle, G., et al. 2012, *ApJ*, 757, 112  
 Casagrande, L., Schönrich, R., Asplund, M., Cassisi, S., Ramírez, I., Meléndez, J., Bensby, T., Feltzing, S. 2011, *A&A*, 530, 138  
 Ciardi, D.R., von Braun, K., Bryden, G., et al. 2011, *AJ*, 141, 108  
 Crepp, J.R., Johnson, J.A., Howard, A.W., et al. 2012, *ApJ*, 761, 39  
 Crepp, J.R., Johnson, J.A., Howard, A.W., Marcy, G.W., Gianninas, A., Kilic, M., Wright, J.T. 2013, *ApJ*, 774, 1  
 Dotter, A., Chaboyer, B., Jevremović, D., Kostov, V., Baron, E., Ferguson, J. W. 2008, *ApJS*, 178, 89  
 Dressing, C.D., Adams, E.R., Dupree, A.K., Kulesa, C., McCarthy, D. 2014, *AJ*, 148, 78  
 Eggleton, P., Kiseleva, L. 1995, *ApJ*, 455, 640  
 Eggenberger, A., Udry, S., Mayor, M. 2004, *A&A*, 417, 353  
 Everett, M.E., Barclay, T., Ciardi, D.R., et al. 2015, *AJ*, 149, 55  
 Girardi, L., Groenewegen, M.A.T., Hatziminaoglou, E., da Costa, L. 2005, *A&A*, 436, 895  
 Guenther, E.W., Hartmann, M., Esposito, M., Hatzes, A.P., Cusano, F., Gandolfi, D. 2009, *A&A*, 507, 1659  
 Harrington, R.S. 1977, *AJ*, 82, 753  
 Hatzes, A.P., Guenther, E.W., Endl, M., Cochran, W.D., Döllinger, M.P., Bedalov, A. 2005, *A&A*, 437, 743  
 Horch, E.P., Howell, S.B., Everett, M.E., Ciardi, D.R. 2014, *ApJ*, 795, 60  
 Holman, M.J., Wiegert, P.A. 1999, *AJ*, 117, 621  
 Howard, A.W., Johnson, J.A., Marcy, G.W., et al. 2010, *ApJ*, 721, 1467  
 Kane, S.R., Howell, S.B., Horch, E.P., et al. 2014, *ApJ*, 785, 93  
 McQuillan, A., Aigrain, S., Roberts, S. 2012, *A&A*, 539, 137  
 Morbey, C.L., Brosterhus, E.B. 1974, *PASP*, 86, 455  
 Musielak, Z.E., Cuntz, M., Marshall, E.A., Stuit, T.D. 2005, *A&A*, 434, 355  
 Raghavan, D., McAlister, H.A., Henry, T.J., et al. 2010, *ApJS*, 190, 1  
 Reffert, S., Quirrenbach, A. 2011, *A&A*, 527, A140  
 Riddle, R.L., Tokovinin, A., Mason, B.D., et al. 2015, *ApJ*, 799, 4  
 Roberts, L.C., Tokovinin, A., Mason, B.D., et al. 2015, *AJ*, 149, 118  
 Tokovinin, A. 2014, *AJ*, 147, 86  
 Tsantaki, M., Sousa, S.G., Santos, N.C., Montalto, M., Delgado-Mena, E., Mortier, A., Adibekyan, V., Israelian, G. 2014, *A&A*, 570, 80  
 van Leeuwen, F. 2007, *A&A*, 474, 653  
 Wang, S.X., Wright, J.T., Cochran, W., et al. 2012, *ApJ*, 761, 46  
 Wang, J., Fischer, D.A., Xie, J.-W., Ciardi, D.R. 2014, *ApJ*, 791, 111  
 Wright, J.T., Howard, A.W. 2009, *ApJS*, 182, 205  
 Wright, J.T., Roy, A., Mahadevan, S., et al. 2013, *ApJ*, 770, 119  
 Zucker, S., Mazeh, T. 2002, *ApJ*, 568, L113